

## Catalytic Behavior of Co/Al<sub>2</sub>O<sub>3</sub> Nanocatalyst under External Magnetic Field

P. Nikparsa<sup>a</sup>, A. Nikparsa<sup>b</sup> and A.A. Mirzaei<sup>a,\*</sup>

<sup>a</sup>Department of Chemistry, University of Sistan and Baluchestan, P. O. Box: 98135-674, Zahedan, Iran

<sup>b</sup>Department of Mechanical Engineering, University of Bojnord, Bojnord 9453155111, Iran

(Received 8 April 2020, Accepted 1 July 2020)

Magnetic behavior of Co/Al<sub>2</sub>O<sub>3</sub> catalyst in Fischer-Tropsch (FT) synthesis is performed using a magnetically fixed bed reactor. X-ray diffraction (XRD) spectroscopy, scanning electron microscope (SEM) method, Brunauer-Emmett-Teller (BET) method, and vibrating sample magnetometer (VSM) method are used to analyze the catalyst. The magnetic field of 0.015 T is suggested for CO hydrogenation on Co/Al<sub>2</sub>O<sub>3</sub> catalyst with fixed bed reactor. The significant effects of magnetic fields are observed in the FT reaction of CO hydrogenation over Co/Al<sub>2</sub>O<sub>3</sub> catalyst. The CO conversion value increases from 78% to 86% at 250 °C with external magnetic field. The apparent activation energy of FT reaction (102.33 kJ mol<sup>-1</sup> without external magnetic field) is reduced (96.45 kJ mol<sup>-1</sup> with applying external magnetic field), and the catalytic activity of Co/Al<sub>2</sub>O<sub>3</sub> catalyst is improved by applying the external magnetic fields during FT process at low temperatures (200-250 °C). The results indicated that the external magnetic fields improved both the rate of reaction and catalytic selectivity to desired hydrocarbons on Co/Al<sub>2</sub>O<sub>3</sub> catalyst.

**Keywords:** Magnetic field effect, Fixed-bed reactor, CO hydrogenation, Activation energy

### INTRODUCTION

Nowadays, the growing demands for liquid fuels and limitations on energy resources have led many researchers to focus on sustainable energy production. FT technology, which is a reaction based on a heterogeneous catalyst between synthesis gas and hydrogen, is a promising process to produce ultraclean synthetic fuels. In terms of industrial and semi-industrial processes, cobalt and iron-based catalysts are commonly used in FT synthesis. Operational costs in this process are an important parameter, especially when FT process is carried out with cobalt-based catalyst. Therefore, researchers have attempted to enhance the operational FT condition to achieve longer life catalysts [1-3]. There are influential factors that have been less studied; for instance, magnetic and electric fields during FT synthesis which will change the reaction process and also the results of experiments [4].

Chemistry is controlled by Coulomb energy; magnetic energy is lower by many orders of magnitude and may be confidently ignored in the energy balance of chemical reactions. The situation becomes less clear, however, when reaction rates are considered. In this case, magnetic perturbations of nearly degenerate energy surface crossings may lead to observable, and sometimes dramatic, effects on reactions rates, product yields, and spectroscopic transitions [5]. The energy levels and chemical reaction rates can also be influenced with magnetic field because of the interaction of the magnetic field with the magnetic dipole moments. This shifts the energy levels and increases the chemical reaction rates because of the Zeeman effect [6]. As far as nanocrystalline solids are concerned, the investigation on the application of the external magnetic field is more attractive because of tuning of spin and charge state during chemical reactions. For instance, the transformation rate of 2,3,5-trimethyl-1,4-hydroquinone to 2,3,5-trimethyl-1,4-benzoquinone and final product yield was increased using the magnetization of nanocatalyst. The adsorption

\*Corresponding author. E-mail: [mirzaei@hamoon.usb.ac.ir](mailto:mirzaei@hamoon.usb.ac.ir)

ability of Cu based nanocatalysts with respect to ammonia was enhanced by applying magnetic field. The results were explained by the magnetic field influence on modifying spin and charge state of Cu-oxide and consequently increasing active centers for the reaction [7]. The magnetic field can also thermodynamically influence the chemical equilibriums, electrode potentials, as well as the electromotive forces [8]. In this study, an external magnetic field is applied on the cobalt-based magnetic particles in a fixed bed reactor during FT synthesis. Additionally, we compare the external magnetic field effects on the FT experiments, selectivity to products, hydrogenation reaction rates, and activation energy. According to the results, applying magnetic field during FT synthesis reduces the activation energy and improves the activity of the Co/Al<sub>2</sub>O<sub>3</sub> nanocatalyst.

## EXPERIMENTS AND METHODS

### Catalyst Preparation

First, Al(OC<sub>2</sub>H<sub>5</sub>)<sub>3</sub> is dissolved in ethanol by vigorously stirring at 60 °C for 30 min. Then, HNO<sub>3</sub> 65% is added to the solution. The mixture is hydrolyzed by adding a H<sub>2</sub>O/C<sub>2</sub>H<sub>5</sub>OH mixture (15/10 cm<sup>3</sup>/cm<sup>3</sup>) and then is stirred to gel for 2 h. After gelation time, the support is dried at 120 °C for 16 h and is calcined at 500 °C for 6 h.

The Co/Al<sub>2</sub>O<sub>3</sub> catalyst is prepared by incipient wetness impregnation of the sol-gel derived Al<sub>2</sub>O<sub>3</sub> (80 wt%) with aqueous Co(NO<sub>3</sub>)<sub>2</sub>·6H<sub>2</sub>O (99% Merck) (2 M) solution. The mixture is rotated for 6 h in a rotaevaporator at 60 °C; after that, it is filtered and dried at 120 °C for 16 h. At the end, the sample is calcined at 500 °C for 6 h.

### Characterization Methods

The BET technique is used to measure the surface areas, pore volumes, as well as the average pore sizes by N<sub>2</sub> physisorption using a Quantachrome Nova 2000 automated system (USA). The magnetic properties are assessed with a vibrating sample magnetometer (IRAN/VSM-4inch) at room temperature. The morphology of sample is observed using a S-360 Oxford scanning electron microscope (SEM) method. For determination of crystalline phases, XRD measurements are carried out using a D<sub>8</sub> advance diffractometer (Bruker AXS, Germany).

### FT Process

The catalytic hydrogenation process is done in a fixed-bed reactor. A schematic representation of the experimental set up is shown in Fig. 1.

In each test run, 1.0 g of the prepared catalyst is held in middle of the reactor using quartz wool. The catalyst is in situ pre-reduced at atmospheric pressure under H<sub>2</sub>/N<sub>2</sub> flow (H<sub>2</sub>/N<sub>2</sub> = 1/1 (flow rate of each gas = 30 cm<sup>3</sup> min<sup>-1</sup>)) at 400 °C for 2 h before the FT reaction. The magneto fixed bed reactor operated with external magnetic fields of 0.015 T. This special fixed bed reactor shows good a performance; it has been designed as a chemical reactor for some scientific research in laboratory. The products are analyzed using a gas chromatograph with two detectors including thermal conductivity detector (TCD) and one flame ionization detector (FID). For each run in a differential reactor, molar flow rate of carbon monoxide in feed is calculated from Eq. (1) [9].

$$F_{CO}^0 = v_0 C_{CO} = \frac{v_0 P_{CO}}{RT} \quad (1)$$

To calculate the consumption rate of CO, the equation of differential reactor is used and consequently the equation of plug reactor was changed as follows:

$$\frac{W_{cat}}{F_{CO}^0} = \int_{X_{CO,in}}^{X_{CO,out}} \frac{dX_{CO}}{-R_{CO}} = \frac{1}{(-R_{CO})_{avg}} \int_{X_{CO,in}}^{X_{CO,out}} dX_{CO} \quad (2)$$

$$= \frac{X_{CO,out} - X_{CO,in}}{(-R_{CO})_{avg}}$$

$$(-R_{CO})_{avg} = \frac{F_{CO}^0 (X_{CO,out} - X_{CO,in})}{W_{cat}} = \frac{F_{CO,out} - F_{CO,in}}{W_{cat}} \quad (3)$$

Thus:

$$\frac{W_{cat}}{F_{CO}^0} = \frac{X_{CO}}{-R_{CO}} \quad (4)$$

Hence:

$$-R_{CO} = \frac{X_{CO} F_{CO}^0}{W_{cat}} \quad (5)$$

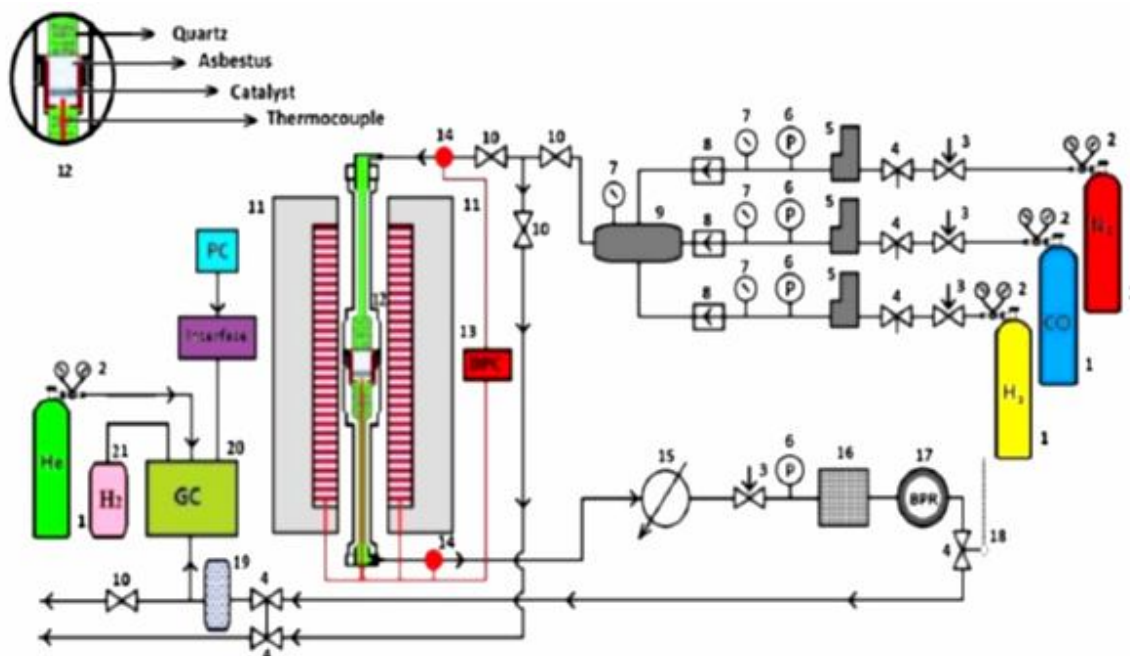


**Fig. 1.** Schematic of reactor for FT reaction, 1-gas cylinders, 2-pressure regulators, 3-needle valves, 4-simple valves, 5-mass flow controllers, 6-digital pressure gauges, 7-pressure gauges, 8-one-way valve, 9-mixing chamber, 10-ball valve, 11-furnace, 12-reaction zone, 13-temperature controller, 14-resistant temperature detector, 15-exchanger, 16-liquid trap, 17-back pressure regulator, 18-flow meter, dewetter, gas chromatograph, hydrogen generator.

**Table 1.** The Results of BET Measurement for the Fresh Calcined Co/Al<sub>2</sub>O<sub>3</sub> Catalyst

Specific surface area (m <sup>2</sup> g <sup>-1</sup> )	Pore volume (cm <sup>3</sup> g <sup>-1</sup> )	Pore size (nm)
108.53	2.45 × 10 <sup>-2</sup>	17.36

In order to minimize the internal mass diffusion resistant, 1.0 g of the catalyst ( $d_p < 60 \mu\text{m}$ ) was powdered and diluted with inert materials (glass wool) to achieve a more uniform bed temperature [10-12].

## RESULTS AND DISCUSSION

### Characterization of the Co/Al<sub>2</sub>O<sub>3</sub> Catalyst

The results of BET measurements of the calcined

sample are present in Table 1. The specific surface area of the Co/Al<sub>2</sub>O<sub>3</sub> catalyst is 108.53; then the prepared catalyst had a good surface area for FT process.

Figure 2 shows the X-ray diffraction patterns (XRD) of the fresh catalyst after calcination. In Fig. 2, the peaks located at  $2\theta$  values are related to different crystal planes of Co<sub>3</sub>O<sub>4</sub>. As shown in Fig. 2, the peak located at  $2\theta$  value of 36.8 is the strongest peak of Co<sub>3</sub>O<sub>4</sub> phase in the XRD spectra corresponding to the (311) plane. In addition, minor

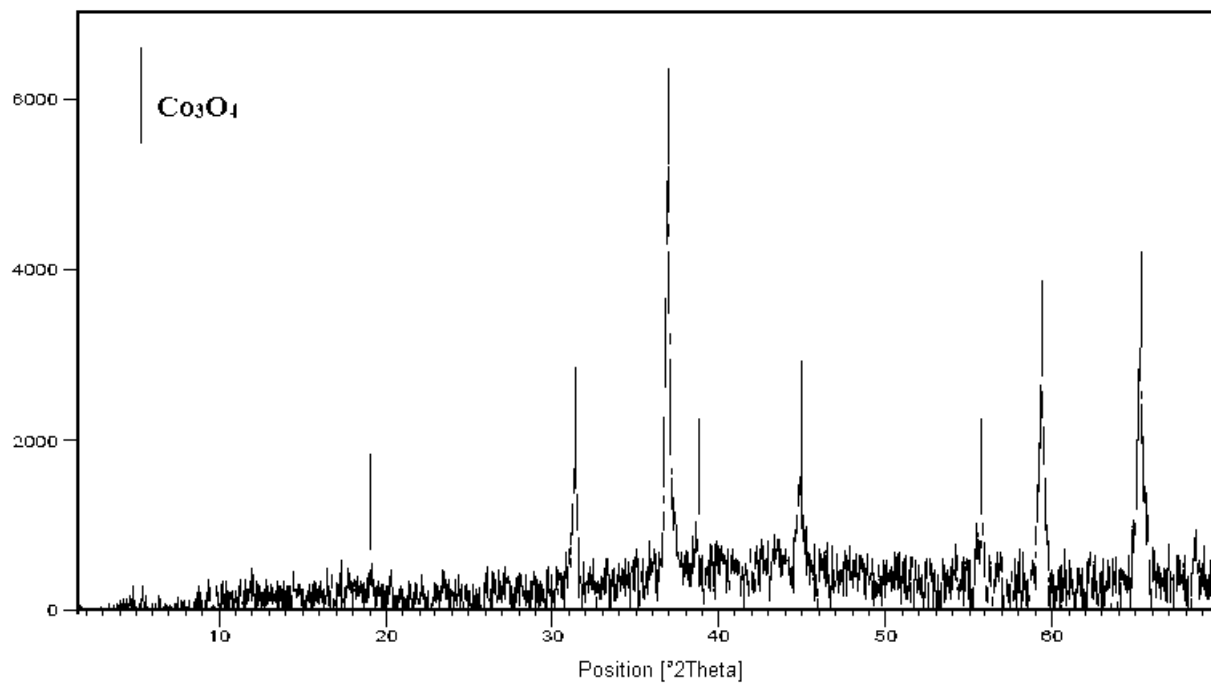


**Fig. 2.** XRD pattern of calcined  $\text{Co}/\text{Al}_2\text{O}_3$  catalyst.

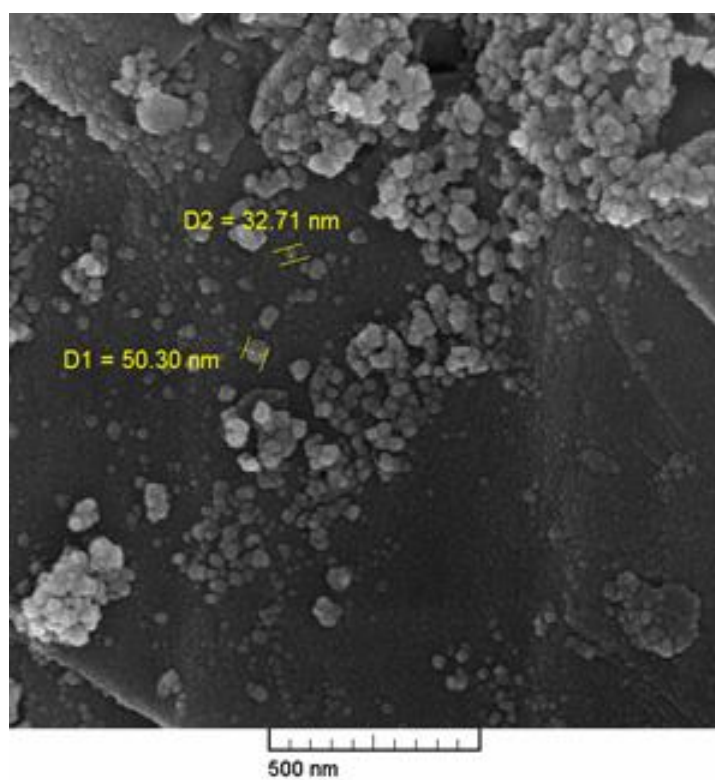


**Fig. 3.** SEM images of the calcined sample.

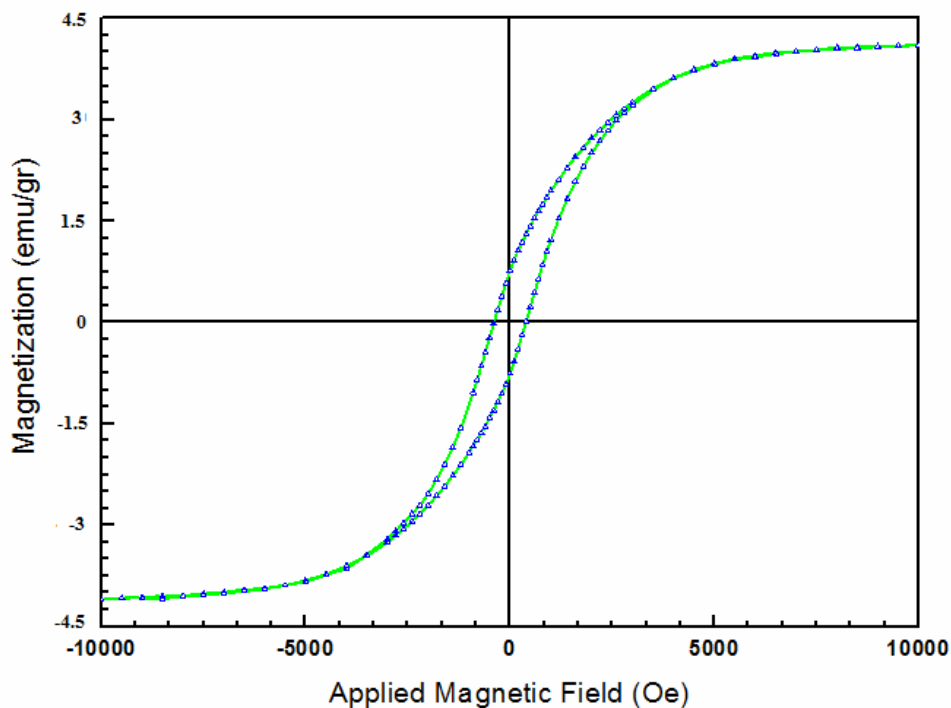


Fig. 4. Magnetization diagrams determined at room temperature for the calcined Co/Al<sub>2</sub>O<sub>3</sub> sample.

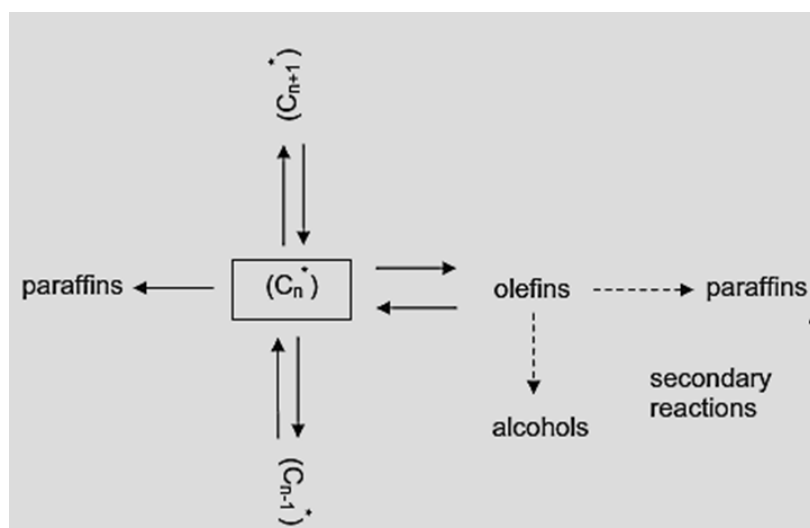


Fig. 5. Illustration of chain growth and termination parameters in the Fischer-Tropsch synthesis [10].

peaks observed at 45 (400), 59 (511) and 65 (440) are correlated with a cubic spinel structure of Co<sub>3</sub>O<sub>4</sub>.

Scanning electron microscopy and selected-area patterns have been used to determine the orientation, size, and

nucleation sites of the calcined catalyst. Figure 3 clearly represents the presence and distributions of nano-sized particles on the surface of Co/Al<sub>2</sub>O<sub>3</sub> sample.

Figure 4 shows magnetic hysteresis loop of the

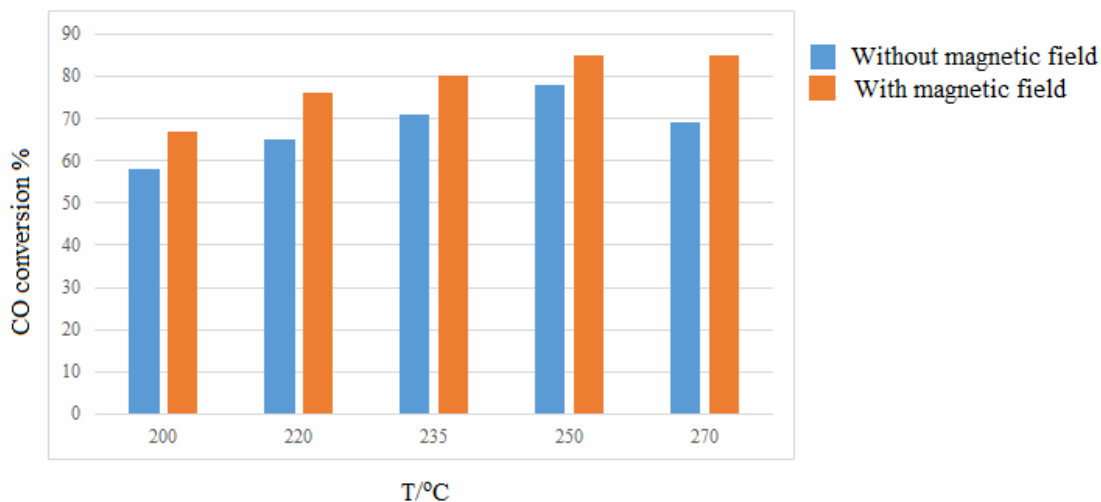


**Fig. 6.** The CO conversion (%) as a function of reaction temperature in FT reaction on Co/Al<sub>2</sub>O<sub>3</sub> catalyst without and with external magnetic field (1 atom, H<sub>2</sub>/CO = 2, 3500 h<sup>-1</sup>).

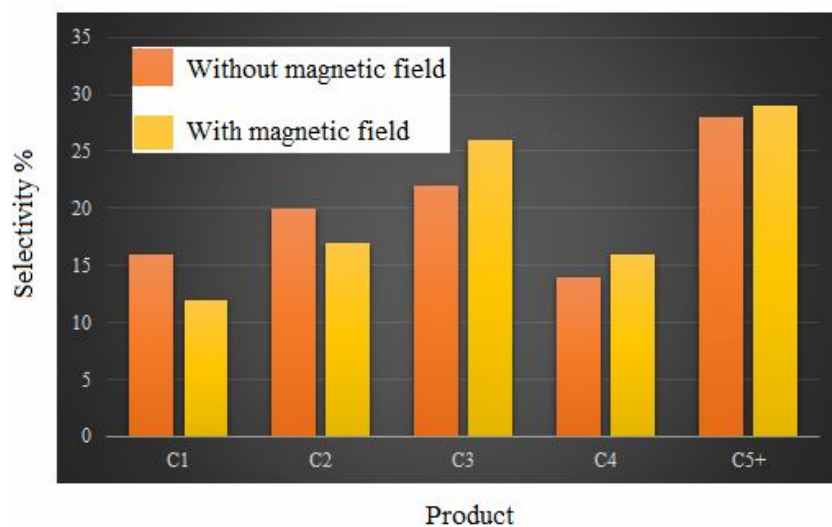


**Fig. 7.** A comparison of the product selectivity obtained from FT reaction on Co/Al<sub>2</sub>O<sub>3</sub> catalyst without and with external magnetic field.

Co/Al<sub>2</sub>O<sub>3</sub> calcined nanocrystalline before the test. As shown, the catalyst is a super paramagnetic compound and its saturation magnetization is about 4.2 emu g<sup>-1</sup>.

### The Effect of Magnetic Field on the Catalytic Performances During FT Reaction

The final FTS products (Fig. 5) are influenced by both

kinds of catalyst samples and operating conditions. Thus, by applying external magnetic field, the carbon selectivity may be affected through structural and/or site/kinetic effects.

Figure 6 compares the results of the Co/Al<sub>2</sub>O<sub>3</sub> catalytic performances with and without the effects of a magnetic field in the fixed bed reactor. This figure shows a good FT results in the presence of the external magnetic field

(0.015 T) at the given operational conditions following: 1 atom, H<sub>2</sub>/CO = 2, and 3500 h<sup>-1</sup>.

The CO conversion values during conventional FT reaction have a rising trend with temperature up to 250 °C (from 58% at 200 °C reaches to 78% at 250 °C), and then they were decreased. This rising trend with temperature can be also observed for the magnetic FT reaction. However, here, the CO hydrogenations have significantly higher values in comparison with the conventional FT reaction.

In Figure 7, the selectivity to products (C<sub>1</sub>, C<sub>2</sub>, C<sub>3</sub>, C<sub>4</sub> and C<sub>5+</sub>) is illustrated for the 20 wt% of Co catalyst during FTS, as well as for the 20 wt% of Co catalyst in the presence of magnetic field at the same operational condition (250 °C, 1 atom, H<sub>2</sub>/CO = 2 and 3500 h<sup>-1</sup>).

The product selectivity for both FT process (without and with external magnetic field) are calculated according to the obtained CO conversion percentages at 250 °C in Fig. 5. As shown, with increasing the percentage of CO conversion in the presence of external magnetic field, the reactivity to methane reduces and the C<sub>3</sub> selectivity increases. There is no very sensible change in the product selectivity to C<sub>5+</sub> with applying the external magnetic field.

The influence of magnetic field on the deactivation rates of Co/Al<sub>2</sub>O<sub>3</sub> catalyst was studied by investigating 75 h time on stream in FT reaction at 230 °C, 1 bar, H<sub>2</sub>/CO mole ratio of 2/1, with GHSV= 1500 h<sup>-1</sup>. The activity versus time-on-stream plot is shown in Fig. 8. The shape curves of two diagrams are nearly similar for reactions. The deactivation kinetic rate can be followed as the equation below [11]:

$$-\frac{dX_{CO}}{dt} = kX_{CO}^n \quad (1)$$

where  $n$  is the degree of reaction and  $k$  is an integral parameter and must be determined for both equations.

As illustrated in Fig. 8, the dip of activity with time could be simulated with power law expressions as follows:

$$-\frac{dX_{CO}}{dt} = kX_{CO}^8 \cdot 10 \quad \text{without external magnetic field} \quad (2)$$

$$-\frac{dX_{CO}}{dt} = kX_{CO}^6 \cdot 84 \quad \text{with external magnetic field} \quad (3)$$

The formulas above indicate that the deactivation rate of Co/Al<sub>2</sub>O<sub>3</sub> catalyst during the process without applying external magnetic field with power orders of 8.10 is higher than that of the process with external magnetic field with 6.84. Consequently, a rapid deactivation rate was observed for the Co/Al<sub>2</sub>O<sub>3</sub> catalyst during conventional FT reaction in 75 h.

### Influence of Magnetic Fields over the Reaction Rate of FTS

The Langmuir-Hinshelwood-Hougen-Watson (LHHW) adsorption theory is a more interesting method for the non-linear FT kinetic study based on cobalt catalysts [11]. The obtained experimental reaction rates are listed in Table 2. To find the best kinetic models, a number of kinetic expressions are accurately tested based on the obtained experimental data. As a result, a model based on the enolic mechanism [3] fits excellently with the experimental CO conversion value at a wide range of operational conditions including 200-250 °C, 1-10 bar, H<sub>2</sub>/CO ratio of 1/1-3/1 and 4200 h<sup>-1</sup>. A schematic of enolic mechanism proposed for Fischer-Tropsch synthesis is presented in Fig. 9.

To facilitate the model discrimination, we consider  $k$  (a kinetic parameter group) as the reaction rate constant and  $a$  (an equilibrium constant group) as the adsorption parameter. The experimental rate of CO consumption fits to the kinetic model below:

$$-r_{CO} = \frac{k P_{CO} P_{H_2}}{(1 + a P_{CO} P_{H_2}^{0.5})^2} \quad (6)$$

The test of the linearized form of the proposed kinetic expression with the experimental data is plotted in Fig. 10. The fitted rate model is also examined using a nonlinear regression based on the obtained experimental data for the catalyst during each process (without and with external magnetic field). The objective function is to minimize the sum of the square of residuals corresponding to a difference between the experimental and theoretical data. The coefficient of determination (R<sup>2</sup>) and the root-mean-square deviation (RMSD) have been reported as a measure of the goodness of fit:

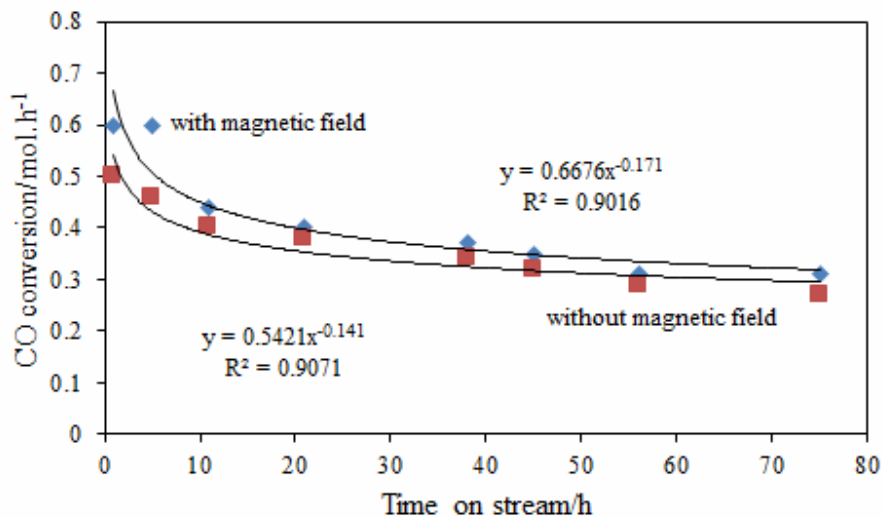


**Fig. 8.** The effect of magnetic field on the deactivation process after 75 h in the FT reaction at 230 °C, 1 bar, H<sub>2</sub>:CO = 2:1, GHSV = 1500 h<sup>-1</sup>.

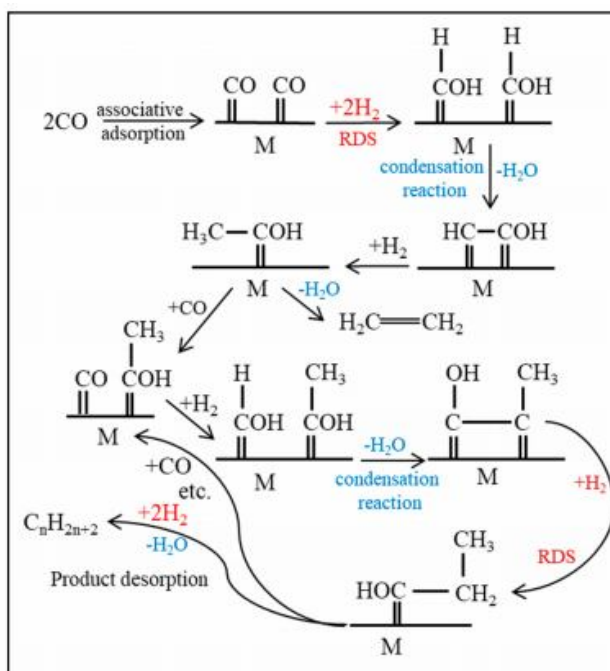


**Fig. 9.** A proposed FTS route based on the enol mechanism.

$$\rho = \frac{1}{N_{\text{exp}}} \sum_{i=1}^{N_{\text{exp}}} r_{\text{CO},i}^{\text{exp}}$$

$$R^2 = 1 - \left( \frac{\sum_{i=1}^{N_{\text{exp}}} (r_{\text{CO},i}^{\text{exp}} - r_{\text{CO},i}^{\text{cal}})^2}{\sum_{i=1}^{N_{\text{exp}}} (r_{\text{CO},i}^{\text{exp}} - \rho)^2} \right)^2 \quad (9)$$

**Table 2.** Comparing the FTS' Reaction Rates in the Presence and Absence of Magnetic Field

T (K)	P <sub>CO</sub> (bar)	P <sub>H<sub>2</sub></sub> (bar)	F <sub>CO</sub> (mol min <sup>-1</sup> )	R1 (mol g <sup>-1</sup> min <sup>-1</sup> )	R2 (mol g <sup>-1</sup> min <sup>-1</sup> )
473.15	1.41	1.41	0.0025	0.0268	0.0301
473.15	1.05	1.05	0.0018	0.0136	0.0158
488.15	0.30	0.30	0.0005	0.0066	0.0009
493.15	0.96	1.44	0.0016	0.0285	0.032
503.15	1.20	1.80	0.0020	0.0285	0.0286
523.15	0.48	0.72	0.0007	0.0106	0.0038
473.15	0.82	1.64	0.0014	0.0266	0.0375

R1: Rate of carbon monoxide in FTS. R2: Rate of carbon monoxide in FTS with external magnetic field.

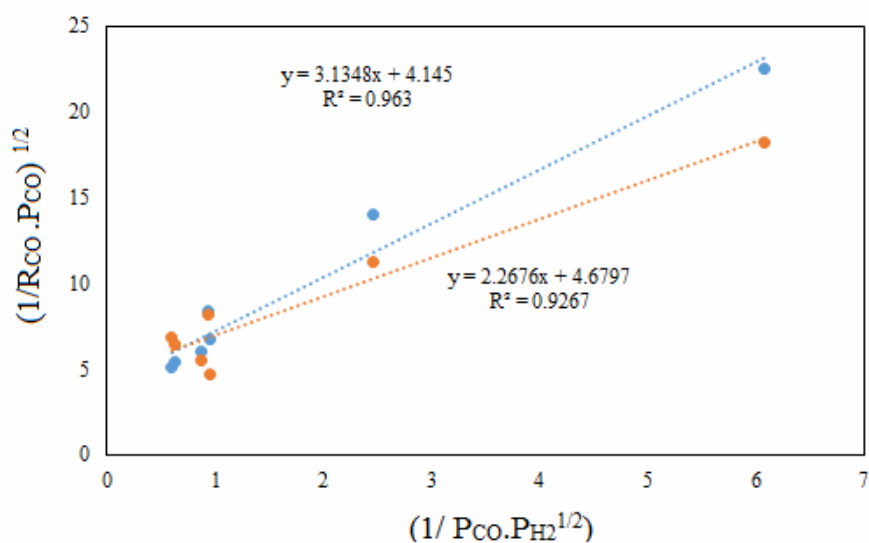


**Fig. 10.** Graphical test of the linearized form of the proposed kinetic rate based on the experimental data of the Co/Al<sub>2</sub>O<sub>3</sub> catalyst. Blue dots indicate the process without magnetic field, and red dots indicate the process with magnetic field.

The RMSD between the experimental and theoretical data is:

$$RMSD = \sqrt{\frac{\sum_{i=1}^{N_{\text{exp}}} (r_{\text{CO},i}^{\text{exp}} - r_{\text{CO},i}^{\text{cal}})^2}{N_{\text{exp}}}} \quad (10)$$

where  $r_{\text{CO},i}^{\text{exp}}$  and  $r_{\text{CO},i}^{\text{cal}}$  are the experimental and theoretical rates and  $N_{\text{exp}}$  clarifies the number of experimental data points with pure error variance  $\rho$ . To investigate the effect of external magnetic field on the kinetic behavior, the

**Table 3.** The Evaluated Kinetic Parameters for the Co/Al<sub>2</sub>O<sub>3</sub> Catalyst (before and after Applying External Magnetic Field) based on the Fitted Kinetic Equation

Parameter	Value		Dimension
	Without magnetic field	With magnetic field	
R <sup>2</sup>	0.95	0.96	-
RMSD	0.00007	0.00007	-
k <sub>0</sub>	6.1 × 10 <sup>8</sup>	2.5 × 10 <sup>8</sup>	-
E <sub>a</sub>	102.33	96.45	kJ mol <sup>-1</sup>

kinetic parameters are evaluated and presented in Table 3. The activation energies of the reaction are achieved based on the Arrhenius equation:

$$k_i(T) = k_i \exp\left(\frac{-E_i}{RT}\right) \quad (11)$$

where k is the rate constant.

As shown in Table 3, the activation energies of the Co/Al<sub>2</sub>O<sub>3</sub> catalyst without and with an external magnetic field are 102.33 and 96.45 kJ mol<sup>-1</sup>, respectively.

The rate constant (*k*) also increased with the external magnetic field. Consequently, the FT rate constant (*k*) increases significantly with applying the external magnetic field, and the reaction rate reduces. Therefore, it could be concluded that with applying the external magnetic field, the rate of reaction increases.

## CONCLUSIONS

In order to investigate the effect of the external magnetic field on the FT reaction results, the CoAl<sub>2</sub>O<sub>3</sub> catalysts are prepared by the sol-gel method. The FT reactions are done in a fixed-bed reactor at a wide range of operational conditions for the catalysts without and with an external magnetic field. The magnetic measurement reveals that the saturation magnetization, *M<sub>s</sub>*, of the Co/Al<sub>2</sub>O<sub>3</sub> catalyst before FT test is more than 4 emu g<sup>-1</sup>. A kinetic model is developed for both catalytic processes within a wide range

of operational conditions based on the enolic mechanism. Kinetic parameters such as kinetic constants (*k*) and activation energies (*E<sub>a</sub>*) for both FT processes are calculated and the results are compared. The overall rate constant (*k*) increases and the apparent activation energy decreases with applying external magnetic field of 0.015 T. It is concluded that the reaction rate increases when an external magnetic field is used for FT reaction. In the case of product selectivity, it is observed that CH<sub>4</sub> selectivity significantly reduces (12%) and the selectivity to the light hydrocarbons (C<sub>2</sub>-C<sub>4</sub>) increases (56%) by applying the magnetic field. In our future studies, a series of iron and cobalt-based catalysts with different magnetization degree will be examined to observe the effect of the external magnetic field on the catalytic behavior during Fischer-Tropsch synthesis.

## ACKNOWLEDGMENTS

The authors gratefully thank University of Sistan and Baluchestan (USB), Iran, for the financial support.

## APPENDIX

### Derivation Rate of Reaction

The reaction rate of the rate-determining step is:

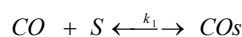
$$-r_{FT} = k_4 \theta_{HOC} \theta_H \quad (1)$$

where  $\theta_{HOC}$  is the surface fraction occupied with the

formyl intermediate and  $\theta_H$  is the surface fraction occupied with the dissociative adsorbed hydrogen. In this model, it is assumed that only surface of HOC occupies a significant fraction of the total number of sites. The fraction of vacant sites,  $\theta_S$ , can be calculated from the following balance equation:

$$\theta_S + \theta_{HOC} = 1 \quad (2)$$

The surface fractions of HOC and H can be calculated from the site balance, the preceding reaction steps which are at quasi-equilibrium:

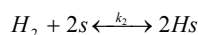


$$k_1 P_{CO} \theta_S - k_{-1} \theta_{CO} = 0 \quad (3)$$

$$\theta_{CO} = K_1 P_{CO} \theta_S \quad (4)$$

$$K_1 = \frac{k_1}{k_{-1}}$$

where  $K_1$  is the equilibrium constant of CO adsorption step.

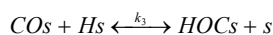


$$k_2 P_{H_2} \theta_S^2 - k_{-2} \theta_H^2 = 0 \quad (5)$$

$$\theta_H = K_2^{0.5} P_{H_2}^{0.5} \theta_S \quad (6)$$

$$K_2 = \frac{k_2}{k_{-2}}$$

where  $K_2$  is the equilibrium constant of dissociated hydrogen adsorption step.



$$k_3 \theta_{CO} \theta_H - k_{-3} \theta_{HOC} \theta_S = 0 \quad (7)$$

$$\theta_{HOC} = \frac{K_3 \theta_{CO} \theta_H}{\theta_S} = K_1 K_2^{0.5} K_3 P_{CO} P_{H_2}^{0.5} \theta_S \quad (8)$$

$$K_3 = \frac{k_3}{k_{-3}}$$

Substituting Eq. (8) into Eq. (2), the concentration of free active site can be expressed as:

$$\theta_S = \frac{1}{1 + K_1 K_2^{0.5} K_3 P_{CO} P_{H_2}^{0.5}} \quad (9)$$

With substituting of Eq. (9) into Eqs. (6) and (8), the expressions of  $[\theta_H]$  and  $[\theta_{HOC}]$  becomes:

$$\theta_H = \frac{K_2^{0.5} P_{H_2}^{0.5}}{1 + K_1 K_2^{0.5} K_3 P_{CO} P_{H_2}^{0.5}} \quad (10)$$

$$\theta_{HOC} = \frac{K_1 K_2^{0.5} P_{CO} P_{H_2}^{0.5}}{1 + K_1 K_2^{0.5} K_3 P_{CO} P_{H_2}^{0.5}} \quad (11)$$

By substituting the surface fraction of HOC and H in Eq. (1), the final rate expression is obtained as follows:

$$-r_{FT} = \frac{k_4 K_1 K_2 P_{CO} P_{H_2}}{(1 + K_1 K_2^{0.5} K_3 P_{CO} P_{H_2}^{0.5})^2} = \frac{k P_{CO} P_{H_2}}{(1 + a P_{CO} P_{H_2}^{0.5})^2} \quad (12)$$

where,  $k$  and  $a$  are kinetic constant and adsorption parameter, respectively.

## REFERENCE

- [1] Li, Z.; Si, M.; Xin, L.; Liu, Re.; Liu, Ru., Cobalt catalysts for Fischer-Tropsch synthesis: The effect of support, precipitant and pH value, *Chin. J. Chem. Eng.* **2018**, *26*, 747-752. DOI: 10.1016/j.cjche.2017.11.001.
- [2] Ershov, M. A.; Potanin, D. A.; Grigorieva, E. V.; Abdellatif, T. M. M.; Kapustin, V. M., Discovery of a high-octane environmental gasoline based on the gasoline Fischer-Tropsch process, *Energy & Fuels*. **2020**, *34*, 4221-4229. DOI: 10.1021/acs.energyfuels.0c00009.
- [3] Shafer, W. D.; Gnanamani, M. K.; Graham, U. M.; Yang, J.; Masuku, C. M.; Jacobs, G.; Davis, B. H., Fischer-Tropsch: Product selectivity-the fingerprint of synthetic fuels, *Catalysts*. **2019**, *9*, 259-315. DOI: 10.3390/catal9030259.

- [4] Westsson, E.; Picken, S.; Koper, G., The effect of magnetic field on catalytic properties in core-shell type particles, *Front. Chem.* **2020**, *8*, 1-9. DOI: 10.3389/fchem.2020.00163.
- [5] Zhang, Z.; Li, Y.; Gu, J.; Ding, L.; Xue, N.; Peng, L.; Guo, X.; Zhu, Y.; Ma, J.; Ding, W., The effect of electrostatic field on the catalytic properties of platinum clusters confined in zeolite for hydrogenation. *Catal. Sci. Technol.* **2018**, *8*, 6384-6395. DOI: 10.1039/C8CY01867G.
- [6] Buchachenko, A.; Lawler, R. G., New possibilities for magnetic control of chemical and biochemical reactions, *Acc. Chem. Res.* **2017**, *50*, 877-884. DOI: 10.1021/acs.accounts.6b00608.
- [7] Rodgers, C. T., Magnetic field effects in chemical systems, *Pure Appl. Chem.* **2009**, *81*, 19-43. DOI: 10.1351/PAC-CON-08-10-18.
- [8] Yermakov, A. Y.; Feduschak, T. A.; Uimin, M. A.; Mysik, A. A.; Gaviko, V. S.; Chupakhin, O. N.; Shishmakov, A. B.; Kharchuk, V. G.; Petrov, L. A.; Kotov, Y. A.; Vosmerikov, A. V.; Korolyov, A. V., Reactivity of nanocrystalline copper oxide and its modification under magnetic field, *Solid State Ion.* **2004**, *172*, 317-323. DOI: 10.1016/j.ssi.2004.05.014.
- [9] Bazubandi, B.; Moaseri, E.; Baniadam, M.; Maghrebi, M.; Gholizadeh, M., Fabrication of multi-walled carbon nanotube thin films *via* electrophoretic deposition process: effect of water magnetization on deposition efficiency, *Appl. Phys. A.* **2015**, *120*, 495-502. DOI: 10.1007/s00339-015-9276-z.
- [10] Marchese, M.; Heikkinen, N.; Giglio, E.; Lanzini, A.; Lehtonen, J.; Reinikainen, M., Kinetic study based on the carbide mechanism of a Co-Pt/ $\gamma$ -Al<sub>2</sub>O<sub>3</sub> Fischer-Tropsch catalyst tested in a laboratory-scale tubular reactor. *Catalysts* **2019**, *9*, 717-736. DOI: 10.3390/catal9090717.
- [11] Iglesia, E.; Reyes, S. C.; Madon, R. J.; Soled, S. L., Selectivity control and catalyst design in the Fischer-Tropsch synthesis: Sites, pellets and reactors, *Adv. Catal.* **1993**, *39*, 221-302. DOI: 10.1016/S0360-0564(08)60579-9.
- [12] Derevich, I. V.; Ermolaev, V. S.; Mordkovich, V. Z.; Solomonik, I. G.; Fokina, A. Y., Heat and mass transfer in Fischer-Tropsch catalytic granule with localized cobalt microparticles, *Int. J. Heat Mass Transf.* **2018**, *121*, 1335-1349. DOI: 10.1016/j.ijheatmasstransfer.2018.01.077